Classical strongly coupled quark-gluon plasma. I. Model and molecular dynamics simulations

Boris A. Gelman, Edward V. Shuryak, and Ismail Zahed
Department of Physics and Astronomy, State University of New York, Stony Brook, New York 11794-3800, USA
(Received 1 February 2006; published 31 October 2006)

We propose a model for the description of strongly interacting quarks and gluon quasiparticles at $T = (1-3)T_c$ as a classical and nonrelativistic colored Coulomb gas. The sign and strength of the interparticle interactions are fixed by the scalar product of their classical *color vectors* subject to Wong's equations. The model displays a number of phases as the Coulomb coupling is increased ranging from a gas, to a liquid, to a crystal with antiferromagnetic-like color ordering. We analyze the model using molecular dynamics simulations and discuss the density-density correlator in real time. We extract pertinent decorrelation times, diffusion, and viscosity constants for all phases. The classical results when extrapolated to the strongly coupled quark-gluon plasma suggest that the phase is liquid-like, with a diffusion constant $D \approx 0.1/T$ and a shear viscosity to entropy density ratio $\eta/s \approx 1/3$.

DOI: 10.1103/PhysRevC.74.044908 PACS number(s): 12.38.Mh, 31.15.Qg, 51.20.+d, 52.27.Gr

I. INTRODUCTION

The quark-gluon plasma (QGP) is a high-temperature phase of QCD. Here, the word *plasma* is used in the same sense as in electrodynamical plasma, that is, a phase with free color charges that are screened [1] rather than confined by the medium. Lattice simulations have shown that the QGP exists above the critical temperature $T_c \approx 170$ MeV in the deconfined and chirally symmetric phase.

Asymptotic freedom of non-Abelian gauge theories ensures that for high enough temperature $T \gg \Lambda_{\rm QCD}$ QGP is *weakly* coupled (wQGP), with particle interactions characterized by a small coupling $\alpha_s(p \approx T) \ll 1$. Weakly coupled QGP is a near-ideal gas of its fundamental constituents, quarks and gluons. Perturbative methods, such as hard thermal loops [2] and other resummation techniques, show how quarks and gluons are dressed and become quasiparticles with T-dependent dispersion curves and widths.

The QGP is experimentally studied using heavy-ion collisions, such as dedicated experiments carried out at the CERN Super Proton Synchrotron during the previous decade and now at the BNL Relativistic Heavy Ion Collider (RHIC). RHIC can reach temperatures of about $2T_c$. The success of the hydrodynamical description for the observed collective flows at RHIC [3] has shown that all dissipative lengths are very short. To produce such flows, the produced matter at RHIC *cannot* be a weakly coupled gas but, at least for some period of time, is a strongly coupled liquid [4].

Recently, two of the authors [5] have suggested that the interaction of quasiparticles in the relevant temperature range at RHIC is strong enough to generate multiple marginal colored Coulomb bound states. Some of those states (charmonium) are observed in current lattice [6] simulations until about $2T_c$. The existence of these states, especially the colored ones, is still debated and warrant further numerical and independent checks on the lattice.

The effective potential energy $U(R)$ of two static colored charges separated by a distance R can also be deduced from lattice simulations. Close to the critical temperature, the separation energy ΔU (the potential at infinity minus its value at some typical distance 0.3 fm) is $\Delta U \approx 1$–4 GeV in the temperature range $T = (1$–$1.2)T_c = 0.17$–0.21 GeV. The ensuing Boltzmann penalty e^{-u} with $u = \Delta U/T \approx 5$–20 is significant, indicating the dominance of potential over kinetic energy. This regime is now called a *strongly* coupled QGP (sQGP). Its structure and consequently its *transport properties* are radically different from a wQGP.

In the context of electromagnetic plasmas, a term "strongly coupled" plasma has a similar meaning. Ionic or dusty plasmas have charged ions with large masses, and thus they are essentially classical. The standard dimensionless parameter characterizing the strength of the interparticle interaction in a classical electromagnetic plasma is the ratio of the potential to the kinetic energy,

$$\Gamma = \frac{(Ze)^2}{a_{\rm WS} T}, \tag{1}$$

where Ze is an ionic charge, $a_{\rm WS} = (3/4\pi n)^{1/3}$ (where n is particle number density) is the Wigner-Seitz radius, and T is the temperature.[1] The dimensionless parameter Γ is convenient because it depends only on *input* parameters, such as the temperature and particle density. However, one should keep in mind that the real interaction parameter is the *output* parameter u,

$$u = \frac{U}{T}, \tag{2}$$

where $U = \langle V \rangle$ is the average interaction of a particle with all its neighbors. This ratio enters the Boltzmann exponent and strongly affects all correlation functions.

Since u is proportional to Γ, one usually defines the weakly coupled regime for $\Gamma \ll 1$ and the strongly coupled regime in the opposite limit $\Gamma \gg 1$. Extensive studies of the one-component plasma (OCP) in electrodynamics, using both molecular dynamics (MD) and analytical methods over the

[1]The Boltzmann constant is $k_B = 1$ so that a temperature has dimension of energy.

past decades, have revealed the following regimes: (i) a gas regime for $\Gamma < 1$, (ii) a liquid regime for $\Gamma \approx 10$, (iii) a glass regime for $\Gamma \approx 100$, and (iv) a solid regime for $\Gamma > 300$. For a review see, for example Ref. [7].

Another physical system closer to what we will discuss in this work is a classical two-component plasma (TCP) with both positive and negative charges. Examples are molten or frozen salts with ions of comparable masses, as in the sQGP. Hydrogen plasmas are better studied, but the underlying charges carry very different masses, so the ensuing results bear no insight into the sQGP where the masses are likely comparable.

Quantum effects will be schematically incorporated in the form of a *localization energy*, providing a repulsive core for the two-particle interaction irrespective of the charge. In the future we plan to study more quantum corrections to classical MD, in particular the role of the exclusion principle and the relation between classically *correlated charges* and quantum bound states.

There are many examples of quantum plasmas. Valence electrons in metals is a well-known example of a quantum plasma. The repulsive nature of the electron-electron interaction excludes the formation of bound states and is very different from QGP. Weak lattice-mediated electron-electron attraction leads to formation of Cooper pairs responsible for superconductivity. Another example of a quantum plasma is a liquid of excitons in semiconductors. Excitons are particle and hole excitations of the Fermi sea with Coulomb attraction between them. In all these cases one needs novel tools to study quantum effects dynamically: The existing ones, such as restricted-path Monte Carlo, use Euclidean time correlators, which (as in the case of lattice QCD) are good for thermodynamical observables but next to impossible to use for transport properties. The approach based on classical molecular dynamics, however crude it may be, is useful tool to study real-time correlators. Some quantum corrections may be added via modification of interaction potentials, as will be briefly discussed in Sec. III.

A model we propose in this paper combines features of strongly coupled Abelian TCP with non-Abelian features of QCD in the form of classical color vectors for the underlying charges. The main interparticle interaction is proportional to the scalar product of the color vectors, which can be attractive, repulsive, or null if the color vectors of the particles are orthogonal to each other. The dynamics of color vectors as well as particle coordinates are described by classical equations of motion (EoM) and can be studied by MD simulations. In Sec. IV we will argue for which values of the parameters this model can be useful for understanding the sQGP.

II. CLASSICAL QUARK-GLUON PLASMA

A. The model

Our classical quark-gluon plasma (cQGP) model is based on the following main assumptions:

(i) The particles are heavy enough to move nonrelativistically, with masses $M \gg T$.

(ii) The interparticle interaction is dominated by colored electric (Coulomb) interactions, with all magnetic effects (such as, e.g., spin forces) ignored.

(iii) The color representations are large, so that color operators t^a can be represented by their average, classical color vectors.

The parameters of the model include the particle mass M and particle density n. The interaction potential is proportional to a scalar product of the unit color vectors times the standard Coulomb interaction strength. Our notation is similar to the convention used in the context of electromagnetic plasmas. The relation between the two is defined by

$$(Z_\alpha e)^2 = C_\alpha \frac{g^2}{4\pi}, \tag{3}$$

where C_α is the eigenvalue of the Casimir operator for $\bar{q}, q, g$.[2]

In QCD all parameters used here are functions of temperature T and the baryon chemical potential μ. In heavy-ion collisions, T and μ are defined by the collision energy and centrality of the collision. Furthermore, for each volume element the cooling of the matter during its expansion is well approximated by the adiabatic (fixed entropy/baryon densities) path on the phase diagram, relating T and μ.

As a first approximation, baryonic charge plays little role at RHIC and thus one can set $\mu = 0$. Hence only one parameter, the temperature T, defines the properties of matter. Therefore, when we attempt to map the MD results for the cQGP into sQGP, all the parameters of the aforementioned model should be converted to temperature, as we will detail. In a way, our classical model will be useful for the sQGP through a one-dimensional slicing of the n-dimensional parameter space. Much like in the case of electromagnetic plasmas, the dimensionless parameter in Eq. (1) is a key in characterizing the transition from a weakly coupled regime with $\Gamma \ll 1$ to a strongly coupled regime with $\Gamma \gg 1$.

At very low temperatures T or very large Γ, any classical system will freeze. Therefore, the low-temperature behavior is dominated by the lowest ordered state. In general, the two-component (Abelian) plasma freezes to an ionic crystal much like ordinary salt (NaCl). The non-Abelian plasma under consideration also has the minimum energy (to which it freezes at $T = 0$) for a *cubic crystal* with *antiferromagnetic* (alternating) order of the classical color vectors. A direction in classical color space is selected randomly, through spontaneous symmetry breaking of the global color group, with alternating directions of the color vectors along the crystal axes.

B. The equations of motion

The Hamiltonian of our model is

$$H = \sum_{\alpha i} \frac{p_{\alpha i}^2}{2m_\alpha} + V_C + V_{\text{core}} \tag{4}$$

[2]Note that the standard notation used in electromagnetism and QCD differ by 4π in the Lagrangian and all subsequent formulas.

with the nonrelativistic kinetic energy. The potential energy is a sum of a color Coulomb interaction V_C and the repulsive core $V_{\rm core}$. The color Coulomb part is

$$V_C = \sum_{\alpha\, i \neq \beta\, j} \frac{Q^a_{\alpha\, i}\, Q^a_{\beta\, j}}{|\vec{x}_{\alpha\, i}, -\vec{x}_{\beta\, j}|}, \tag{5}$$

where the sum is over the species $\alpha = q, \overline{q}, g$ and their respective numbers $N_\alpha i$. There is also a summation over the color indexes a. We will specify $V_{\rm core}$ in the following.

Thus our phase-space coordinates are the positions (x_α), momenta (p_α), and color (Q_α). The latter rotates under global gauge transformation with a matrix

$$Q^a \to D^{ab}(\Lambda)\, Q^b, \tag{6}$$

which makes Eq. (5) gauge invariant. Only the Coulomb-like interaction is retained in Eq. (5) since magnetically induced interactions are subleading in the nonrelativistic limit. This is the case for all spin and local many-body forces. For instance the standard non-Abelian three-gluon interaction

$$\sum_{\alpha\, i \neq \beta\, j \neq \gamma\, k} Q^a_{\alpha_i}\, Q^b_{\beta_j}\, Q^c_{\gamma_k}\, (f^{abc}\vec{F}) \tag{7}$$

is subleading $\vec{F} \approx \vec{\nabla}/m$ since at least one of the gluons must be magnetic. Nonlocal many-body interactions induced by the two-body Coulomb and core interactions are important and are "resummed" by solving the EoM to all orders using MD.

The EoM for the phase-space coordinates follow from the usual Poisson brackets. For the standard coordinates they are

$$\left\{x^m_{\alpha\, i},\, p^n_{\beta\, j}\right\} = \delta^{mn}, \delta_{\alpha\beta}\delta_{ij}, \tag{8}$$

and for the color coordinates they are

$$\left\{Q^a_{\alpha\, i},\, Q^b_{\beta\, j}\right\} = f^{abc}\, Q^c_{\alpha\, i}. \tag{9}$$

Equation (9) is the classical analog of the SU(N_c) color commutators, where f^{abc} are the structure constants of the color group. The classical color vectors are all adjoint vectors with $a = 1, \ldots, (N_c^2 - 1)$. The difference between quarks and gluons follow from their respective Casimir operators.

The color vectors Q^a are not the canonical coordinates. A canonical phase-space description requires the use of the Darboux parameterization [8]

$$Q = (\Phi^A, \Pi^A), \tag{10}$$

with $A = 1, .., N_c(N_c - 1)/2$ satisfying standard canonical commutation relations

$$\{\Phi^A, \Pi^B\} = \delta^{AB}, \tag{11}$$

where $\Phi' s$ are angular coordinates and the $\Pi' s$ are angular momenta. The $\Pi' s$ are identified with the fixed Casimirs of SU(N_c), which are conserved by the equations of motion. For example, for $N_c = 2$, the conserved operator is a Casimir C_2 (the length of a color vector). Without loss of generality, the Darboux coordinates may be chosen as

$$(Q_1 \pm i\, Q_2,\, Q_3) = (\sqrt{J^2 - \Pi^2}\, e^{\pm i\Phi},\, \Pi), \tag{12}$$

with $J^2/3 = C_2$. For $N_c = 3$ the color vectors are eight dimensional, with two conserved Casimirs $(Q^a Q^a)$ and $(d^{abc} Q^a Q^b Q^c)$ and six variables. In this case, the Darboux set is more involved but can be parametrized with three angles and three conjugate momenta. We will not use the Darboux coordinates.

The equations of motion for our classical Coulomb gas follow from Eqs. (4), (8), and (9):

$$\begin{aligned} \dot{x}^n_{\alpha\, i} &= \left\{H,\, x^n_{\alpha\, i}\right\} = \frac{p^n_{\alpha\, i}}{m_\alpha}, \\ \dot{p}^n_{\alpha\, i} &= \left\{H,\, p^n_{\alpha\, i}\right\} = g\, E^{an}_{\alpha\, i}\, Q^a_{\alpha\, i}, \\ \dot{Q}^a_{\alpha\, i} &= \left\{H,\, Q^a_{\alpha\, i}\right\} = g\, f^{abc}\, Q^b_{\alpha\, i}\, A^c_{\alpha\, i\, 0}, \end{aligned} \tag{13}$$

where

$$\begin{aligned} \vec{E}^a_{\alpha\, i} &= -\vec{\nabla}_{\alpha\, i}\, A^a_{\alpha\, i\, 0} \\ &= -\vec{\nabla}_{\alpha\, i} \sum_{\beta\, j \neq \alpha\, j} \frac{g\, Q^a_{\beta\, j}}{|\vec{x}_{\alpha\, i} - \vec{x}_{\beta\, j}|}. \end{aligned} \tag{14}$$

The three equations in (13) are also known as Wong's equation [9]. Owing to the antisymmetric nature of the structure constant f^{abc}, it has the form of rotation of the color vector that conserves its length (classical precession).

III. NUMERICAL STUDIES USING MOLECULAR DYNAMICS

A. An interaction potential and units

The MD simulation is a numerical solution of the EoM [Eq. (13)] starting from some initial conditions for fixed number of particles contained in a cubic box of a given volume. The method was originally developed to study properties of classical liquids and plasmas. It is the most straightforward way to access transport properties such as the diffusion coefficient D, and the shear viscosity η, and the heat conductivity λ.

In a typical MD simulation of a two-component electromagnetic plasma the interparticle potential is chosen as

$$V(r) = V_{\rm core} + V_C = \left(\frac{(Ze)^2}{\lambda}\right)\left[\frac{1}{n}\left(\frac{\lambda}{r}\right)^n + \frac{Q_i Q_j}{r}\right], \tag{15}$$

with $r = |\vec{x}_i - \vec{x}_j|$ and where $Q_i, Q_j = \pm 1$ are electric charges. The repulsive potential $V_{\rm core}$ (with $n \geqslant 2$) ensures that the system is stable against a collapse. For systems such as NaCl Hansen and McDonald [10] used a repulsive core with $n = 9$. For these molten salts the core follows from the intrinsic repulsion of the atomic electrons.

Since we are interested in understanding the role played by the non-Abelian color charges, we have carried the MD analysis for both the Abelian and non-Abelian cases. In this paper we report the results of MD simulations for the SU(2) color group. In this case quarks and gluons have equal Casimirs, $C_q = C_g$ We used the same form of $V_{\rm core}$ in the non-Abelian simulation as in the Abelian case.

The microscopic motivation in QCD for $V_{\rm core}$ stems from the short-range part of the interparticle interactions. Needless to say, this is a complex problem, and not much is known about it from first principles, whether in the intermediate coupling region ($\alpha_s \approx 1/2$) or in the very strong coupling region ($\alpha_s \approx 1$ or $\Gamma \gg 1$).

One reason for an effective repulsion at short distances is due to the kinetic energy of the quantum localization. Such repulsion can be modeled by a repulsive potential of the form

$$V_{\rm loc} \approx \frac{\hbar^2}{mr^2}. \tag{16}$$

Such potentials are often used in classical simulations of light atoms (e.g., solid He). Note that this term has a power $n = 2$ rather than the $n = 9$ used in $V_{\rm core}$. This is not very important since any $n > 1$ stabilizes the Coulomb attraction at short distances. The net effect of the quantum localization is the introduction of a dimensionful parameter (i.e., $\hbar$ in natural classical units).

In our analysis we used the following *natural* units.

(i) Length unit: At any n, the minimum of the potential is at $r = \lambda$. So λ sets the basic length scale, and all distances are measured in units of λ.

(ii) Time unit: The unit of time τ_0 will be set by the natural frequency of a screened Coulomb system, its plasma frequency

$$\tau_0 = \omega_p^{-1} = \left(\frac{m}{4\pi n e^2}\right)^{1/2}. \tag{17}$$

(iii) Mass unit: This is naturally given by the particle mass m. Thus all important time correlators have a characteristic length of order 1 in τ_0. In contrast, all MD runs are typically a few hundreds or thousands of τ_0 to ensure statistical equilibrium.

This fixes the three basic units used in our analysis. For instance, the kinetic energy is measured in obvious units of $m\lambda^2/\tau_0^2$. The strength of the Coulomb potential, if measured in such units, is

$$\left(\frac{e^2}{\lambda}\right) \Big/ \left(\frac{m\lambda^2}{\tau_0^2}\right) = \frac{1}{4\pi}\frac{1}{n\lambda^3}, \tag{18}$$

so that it is defined directly by the particle density. The temperature, in the same units, can be defined via averaged (dimensionless) velocities as $(3/2)T = \langle v^2/2\rangle$. Finally, the main parameter u in Eq. (2) can be obtained from simulation, as the ratio of the *measured* total mean potential to the total kinetic energy.

B. Technical details

There are readily available numerical packages for solving a set of coupled differential equations of the type listed in Eq. (13). The accuracy is tested through energy conservation and color vectors remaining on the unit sphere. We have used the package from the CERN library in double precision and tested its accuracy for both energy and color conservation.

A many-body problem of particles in a box requires boundary conditions. We used periodic boundary conditions. When a particle crosses one side of a box, it reappears on the opposite side with the same velocity. We can visualize space as filled with many mirror cubes, next to each other. When one particle leaves the central cube, its mirror image enters from the opposite cube. The interparticle potential in this many-cube world is periodic under cubic translation by $\vec{L}$, that is,

$$V_{ij} = \sum_{n_x,n_y,n_z=-\infty}^{+\infty} V(\vec{x}_i - \vec{x}_j + n\vec{L}). \tag{19}$$

When a particle crosses the boundary, there is no change in the force or the potential since Eq. (19) is truly periodic. In practice, the sum in Eq. (19) is carried over a few adjacent cubes or mirror images, causing an overall loss of periodicity. As a result, the forces at the faces of the cube jump slightly, thereby causing random kicks on the crossing particles. This effect gradually heats the system. The longer the range of the potential is, the more severe is the heating. However, modern computers easily allow for keeping up to 3–4 mirror images on each side of a central cube, thereby reducing the net electric field by orders of magnitude[3] and solving this problem.

Another practical way to deal with this problem is to introduce a very small amount of friction into the EoM, which can compensate the heating effect caused by the random forces at the cubic interface. Our typical runs consists of $4^4 = 64$ or $6^4 = 1296$ particles all of the same species. The results discussed in the following are for 64 particles.

C. Structure factor

The static and dynamic properties of a liquid are determined by various correlation functions. One of the most useful of these functions is a density-density correlation function or structure factor, defined as

$$G(r,t) = \frac{1}{n}\langle\rho(\vec{x},t)\rho(\vec{0},0)\rangle, \tag{20}$$

where $r = |\vec{x}|$, $n = N/V$ (with N the number of particles and V the volume of the box), and $\rho(\vec{x},t)$ is a microscopic particle density function at the position $\vec{x}$ at time t, given by

$$\rho(\vec{x},t) = \sum_{i=1}^{N} \delta(\vec{x} - \vec{x}_i(t)), \tag{21}$$

where $\vec{x}_i(t)$ is the position of the ith particle at time t. The averaging in Eq. (22) is carried over an equilibrium ensemble.[4]

By assuming translational invariance and isotropy, the classical density-density correlation function can be written as

$$G(r,t) = \frac{1}{N}\left\langle \sum_{i=1}^{N}\sum_{j=1}^{N} \delta[\vec{x} + \vec{x}_i(0) - \vec{x}_j(t)] \right\rangle. \tag{22}$$

The time-dependent structure function $G(r,t)$ characterizes the likelihood to find the jth particle at the position $\vec{x}_j$ at time

[3]Traditionally the Bethe polynomials for Ewald sums are used to overcome this heating phenomenon caused by the truncation. We have found this procedure to be less accurate for the amount of complexity it introduces.

[4]Since in our MD simulation the total energy and number of particles of a system are kept constant this corresponds to using a microcanonical ensemble.

t if particle j was at the position $\vec{x}_i$ at $t = 0$. This structure function is referred to as the van Hove correlation function.

The density-density correlation function (22) can be written as a sum of two parts: a *self-correlation*G_s and a *distinct-correlation*G_d,

$$G(\vec{x}, t) = G_s(\vec{x}, t) + G_d(\vec{x}, t), \tag{23}$$

where

$$G_s(\vec{x}, t) = \frac{1}{N}\left\langle \sum_{i=1}^{N} \delta(\vec{x} + \vec{x}_i(0) - \vec{x}_i(t)) \right\rangle \tag{24}$$

and

$$G_d(\vec{x}, t) = \frac{1}{N}\left\langle \sum_{i\neq j}^{N} \delta(\vec{x} + \vec{x}_i(0) - \vec{x}_j(t)) \right\rangle. \tag{25}$$

We have such functions for different values of the dimensionless constant Γ. In Fig. 1 we show the functions G_d at three values of the coupling: moderate, strong, and very strong, $\Gamma = 0.83, 31.3$, and 131, respectively The first case shows a relatively weak correlation between the particles, at distance 1 (in our units) corresponding to the potential minimum, which relaxes rather quickly with time. The correlation is more robust in the second ("liquid") case and is very stable and is accompanied by extra peaks in a "solid" case.

D. Transport coefficients

An important aspect of the strongly coupled plasmas is the dramatic change in transport properties in comparison to weakly coupled plasmas. MD simulations can be used to study the transport properties at strong coupling, in particular, the shear and bulk viscosities, diffusion constant, thermal conductivity, and color conductivity. A simple way to obtain these transport coefficients is via the Green-Kubo relations. These relations give the transport coefficients in terms of the integrals of the equilibrium time-dependent correlation functions.

For self-diffusion the corresponding correlation function is the velocity autocorrelation function,

$$D(\tau) = \frac{1}{3N}\left\langle \sum_{i=1}^{N} \vec{v}_i(\tau)\cdot\vec{v}_i(0) \right\rangle, \tag{26}$$

where $\vec{v}_i(\tau)$ is the velocity of a particle i at time τ. The velocity autocorrelation functions are shown in Fig. 2 for $\Gamma = 0.83, 31.3$, and 131, respectively. This refers to the nonideal gas, liquid, and crystal of the (one-species) cQGP.

The diffusion constant is the integral of the velocity autocorrelation function,

$$D = \int_0^\infty D(\tau)d\tau. \tag{27}$$

Figure 3 shows a log-log plot of the diffusion constant as a function of Γ. The dependence of D on $\log\Gamma$ is linear and can be approximately described by a simple power,

$$D \approx \frac{0.4}{\Gamma^{4/5}}. \tag{28}$$

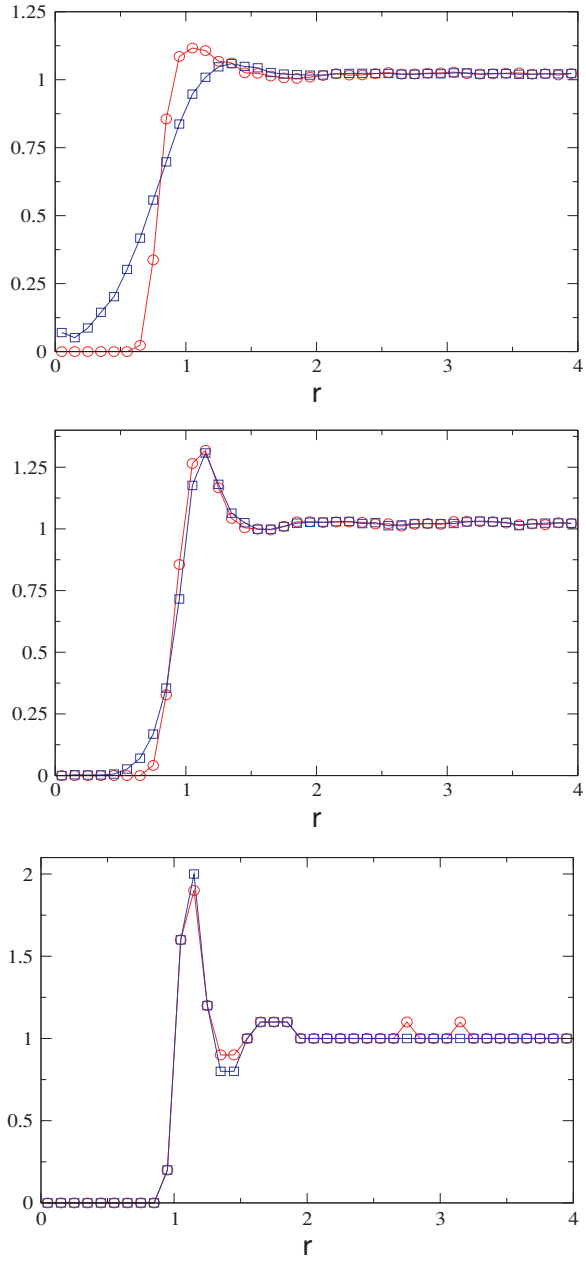

FIG. 1. (Color online) G_d correlation function for (top to bottom) $\Gamma = 0.83, 31.3$, and 131, respectively. Red circles correspond to $t^* = 0$, and blue squares correspond to $t^* = 5$. Here and in the following all quantities are in units defined in Sec. III A.

The viscosity coefficients are given in terms of time autocorrelation function of the stress-energy tensor,

$$\eta(\tau) = \frac{1}{3TV}\left\langle \sum_{x<y} \sigma_{xy}(\tau)\sigma_{xy}(0) \right\rangle, \tag{29}$$

where $\sum_{x<y}$ denotes a sum over the three pairs of distinct tensor components (xy, yz, and zx). The off-diagonal parts of the stress-energy tensor are given by

$$\sigma_{xy} = \sum_{i=1}^{N} m_i v_{ix} v_{iy} + \frac{1}{2}\sum_{i\neq j} r_{ij,x} F_{ij,y}, \tag{30}$$

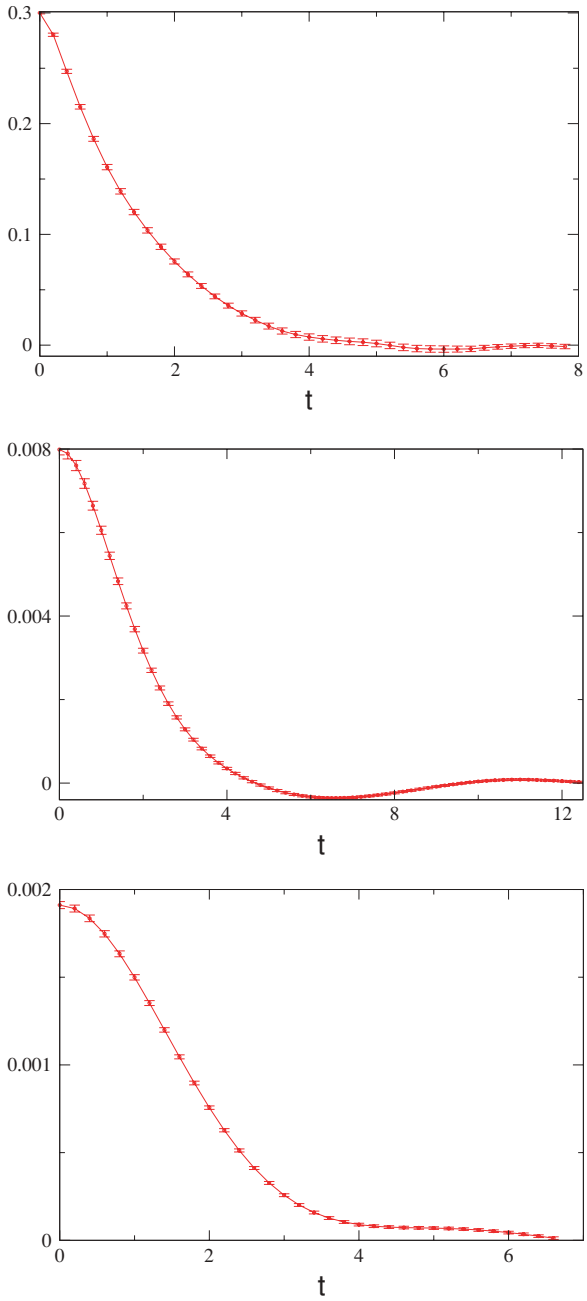

FIG. 2. (Color online) Velocity autocorrelation function $D(t)$ for (top to bottom) $\Gamma = 0.83$, 31.3, and 131, respectively.

and similarly for xz and yz, with $\vec{r}_{ij} = \vec{x}_j - \vec{x}_i$ and where $\vec{F}_{ij}$ is the force on particle i due to particle j. The stress-tensor autocorrelation functions are shown in Fig. 4 for $\Gamma =$ 0.83, 31.3, and 131, respectively.

The Green-Kubo relation for the coefficient of the shear viscosity is

$$\eta = \int_0^\infty \eta(\tau) d\tau. \tag{31}$$

The coefficient of shear viscosity as a function of Γ is shown in Fig. 5. For small Γ the viscosity is large since the mean-free path is large in a gaslike phase. The viscosity has a minimum in the liquid phase and rises slowly as Γ increases. The coefficient η can be approximately written as

$$\eta \approx 0.001\Gamma + \frac{0.242}{\Gamma^{0.3}} + \frac{0.072}{\Gamma^2}. \tag{32}$$

The minimum measured viscosity is $\eta \approx 0.1$ at $\Gamma \approx 10$.

The stress-tensor autocorrelation function can be used to determine the viscous decorrelation time τ_η, defined as

$$\tau_\eta = \frac{\eta}{\eta(0)}, \tag{33}$$

where $\eta(0)$ is the value of the stress-energy autocorrelation function at time $t = 0$. The values of $\eta(0)$ and τ_η as a function of Γ are shown in Figs. 6 and 7, respectively.

The functional dependence on Γ of $\eta(0)$ is approximately given by

$$\eta(0) \approx 0.0005\Gamma + \frac{0.77}{\Gamma^{1.57}} + \frac{0.44}{\Gamma^{0.33}}. \tag{34}$$

and that of the decorrelation time by

$$\tau_\eta \approx 0.239 + 0.091\sqrt{\Gamma}. \tag{35}$$

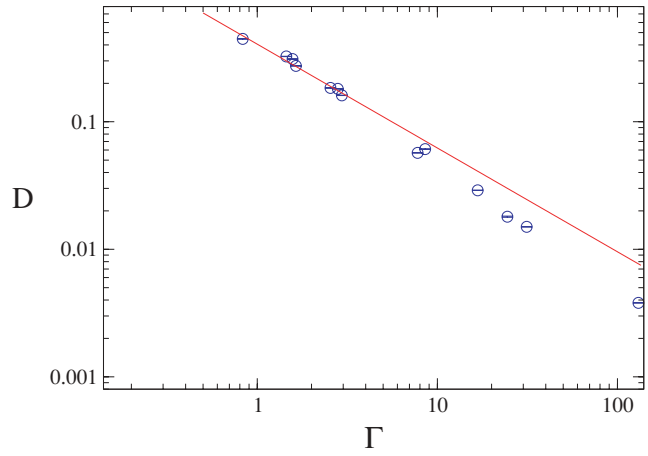

FIG. 3. (Color online) The diffusion constant D as a function of the dimensionless coupling Γ. Blue points are the MD simulations; the red curve is the expression (28).

E. Potential energy

Another useful observable that can be determined using MD simulations is the total potential energy U divided by NT. This ratio as a function of Γ is shown in Fig. 8. The parametric dependence of this ratio on Γ is approximately given by

$$\frac{U}{NT} \approx -4.9 - 2\,\Gamma + 3.2\Gamma^{1/4} + \frac{2.2}{\Gamma^{1/4}}. \tag{36}$$

At large Γ the crystal phases sets in, and the potential energy asymptotes as $U/NT \approx -2\Gamma$, which is a measure of the Madelung constant. A full theoretical analysis of Eq. (36) will be given in a subsequent paper [11].

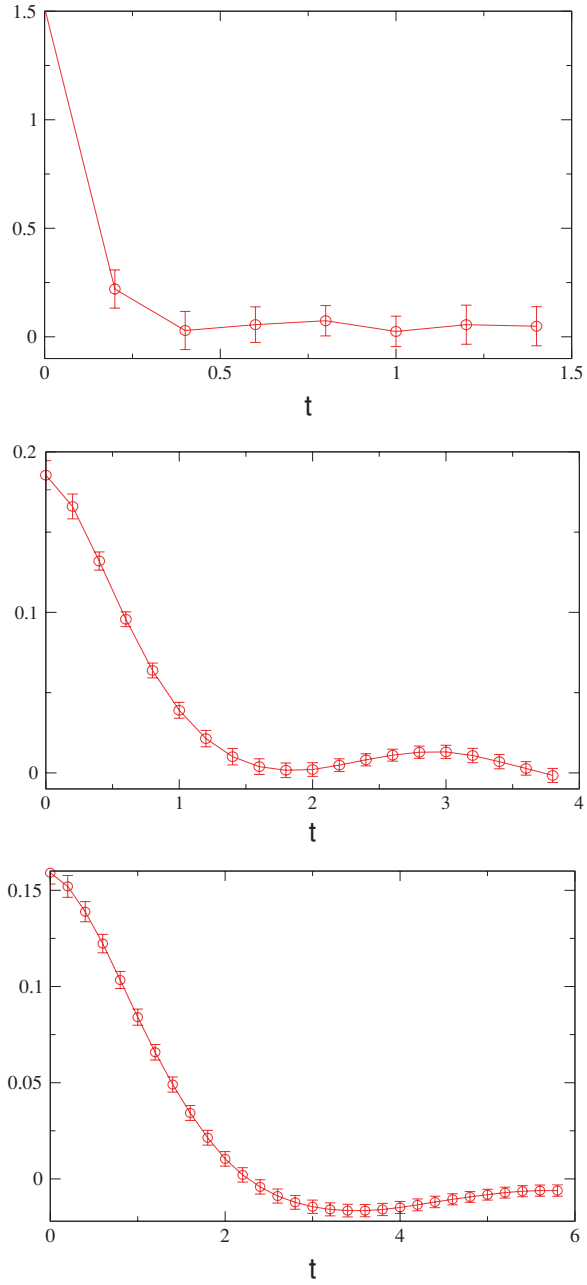

FIG. 4. (Color online) Stress-tensor autocorrelation function $\eta(\tau)$ for (top to bottom) $\Gamma = 0.83$, 31.3, and 131, respectively.

IV. COMPARISON WITH STRONGLY COUPLED QGP

A qualitative mapping of the one-species cQGP described here into sQGP can be made by adjusting the three basic scales described in Sec. III, namely those of the length, the time, and the mass. As we have already indicated, all parameters of the model are functions of the temperature T of the sQGP. In this section we use heuristic arguments to obtain values of these parameters for temperatures $T = (1.5\text{–}3)T_c$. (It is used as a reference point because more lattice data are available for it than for T close to T_c.)

As previously discussed, the unit of length λ is the minimum of the potential. Since the repulsive part mocks up the quantum

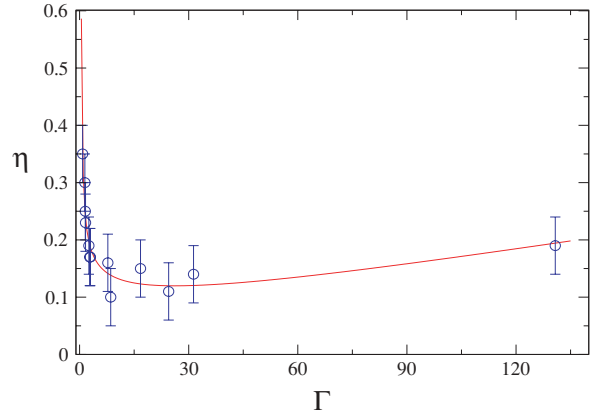

FIG. 5. (Color online) Shear viscosity η as a function of the dimensionless coupling Γ. Blue points are the MD simulations; the red curve is the fit in Eq. (32).

repulsion at short distances, the effective interparticle potential is[5]

$$V_{\text{eff}} = \frac{\hbar^2}{2mr^2} - \frac{C\,\alpha_s}{r}, \tag{37}$$

with a minimum at $r_0 = \hbar^2/(mC\alpha_s) = \lambda$. C is the Casimir operator for quarks and gluons.

The quasiparticle mass, defined as its energy at zero momentum, is at $T = (1.5\text{–}3)T_c$ about constant $m \approx 5T_c$ both for quark and gluon quasiparticles [12]. We note that there are no direct lattice measurements of quasiparticle dispersion curves below $1.5\,T_c$. One can infer quark quasiparticle masses from fits to thermodynamical observables and baryonic susceptibilities. These fits show that masses grow toward T_c. (For a recent discussion see Ref. [13].)

It is convenient to introduce a dimensionless mass parameter $\tilde{m} = m/T$, which thus changes from large values close to T_c

[5]Insofar as our discussion was classical and nonrelativistic, both $\hbar$ and $1/c$ were set to zero. In this section, and this section only, we use the standard high-energy units with $\hbar = 1$, $c = 1$.

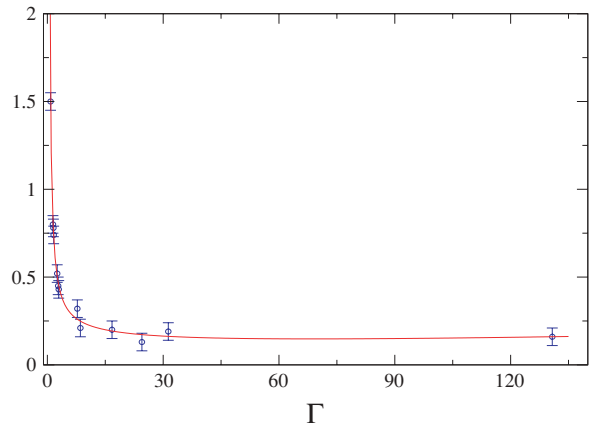

FIG. 6. (Color online) Stress-energy autocorrelation function at $t = 0$, $\eta(0)$, as a function of Γ. The blue points are the MD simulations; the red curve is the fit of Eq. (34).

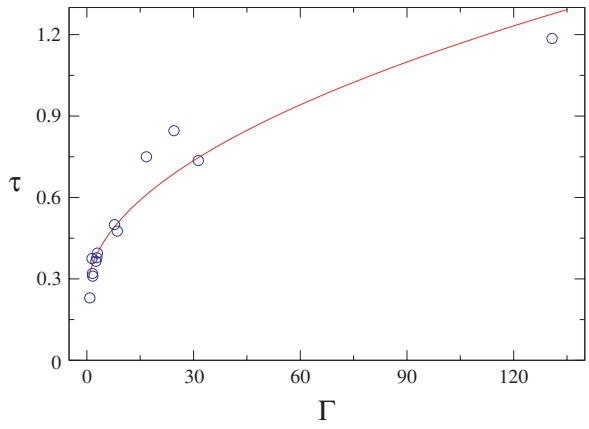

FIG. 7. (Color online) The viscous decorrelation time τ_η as a function of Γ. The blue points are the MD simulations; the red curve is the fit in Eq. (35).

to about 3 at $1.5T_c$. Clearly, its value determines the accuracy of the nonrelativistic approximation. For example, at $\tilde{m} = 5$ the mean square momentum $\sqrt{\langle p^2 \rangle}/T = 4.8$ if calculated relativistically, whereas the nonrelativistic approximation gives a value smaller by a factor of 0.8. The corresponding ratio of the total density in the nonrelativistic approximation is 0.7 of its relativistic value. So, it is not an unreasonable approximation, but it is not very accurate. At $T = 1.5T_c, \tilde{m} \approx 3$ only, with even worse accuracy. Therefore, we should calculate momentum integrals relativistically, and only the results should be mapped into cQGP.

The Casimir operators for gluons $C_g = 3$ and quarks $C_q = 4/3$ should be averaged over their respective weights. The number of effective degrees of freedom in thermodynamical quantities is such that roughly all three species—$g, \bar{q}, q$—are equally represented. Furthermore, the values of the coupling constant α_s inferred from measured static potentials at relevant distances is $\alpha_s \approx 0.5$. Within the uncertainties we use

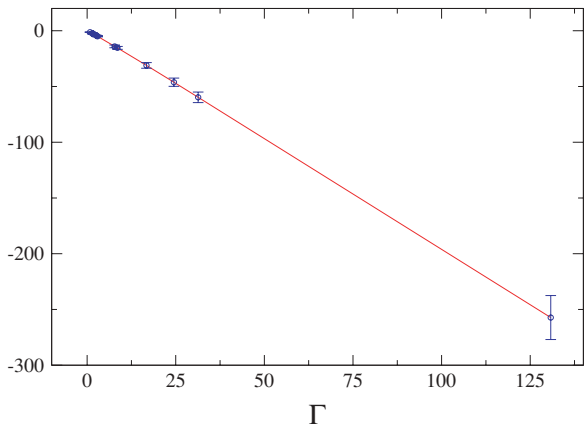

FIG. 8. (Color online) Ratio of the total potential energy U to NT as a function Γ. The blue points are the MD simulations; the red curve is the fit in Eq. (36).

$\langle \alpha_s C \rangle = 1$. Thus,

$$\lambda = r_0 \approx \frac{1}{3T}. \tag{38}$$

The density of quasiparticles n can be estimated as follows. Although quasiparticles are relatively heavy, the presence of light bound states increases the total density of quasiparticles to about 0.8 of the entropy density per particle in the massless gas [14]. Ignoring this 0.8, which refers to the bound states, we then have

$$n \approx (0.244T^3)\,(8 + 6\,N_f) \approx 6.3T^3, \tag{39}$$

where the first term in parentheses is the usual density of blackbody radiation photons, and the second is the number of effective degrees of freedom from the eight colored gluons and two quarks and antiquarks with three colors and N_f flavors. This corresponds to the following Wigner-Seitz radius:

$$a_{\rm WS} = \left(\frac{3}{4\,\pi\,n}\right)^{1/3} \approx \frac{1}{3T} \approx \lambda. \tag{40}$$

The time units in MD are given by the plasma frequency, which is

$$\tau_0 = \omega_p^{-1} = \left(\frac{4\pi n \langle \alpha_s\, C \rangle}{m}\right)^{-1} \approx \frac{1}{5.1T}, \tag{41}$$

where, for definiteness, we used $m = 3T$.

In summary, our MD results for cQGP can be qualitatively translated to the dimensionfull sQGP parameters using, respectively, the length λ, time τ_0, and mass m units

$$\begin{aligned} \lambda &\approx \frac{1}{3\,T}, \\ \tau_0 &\approx \frac{1}{5.1\,T}, \\ m &\approx 3\,T, \end{aligned} \tag{42}$$

with $\Gamma \approx 3$.

Indeed, the viscosity unit η_0 is then given by the combination of units with the appropriate dimensions:

$$\eta_0 = m/(\tau_0\,\lambda) = (3T)(5.1T)(3T) \approx 46T^3, \tag{43}$$

leading to the sQGP viscosity through

$$\eta \to \eta\,\eta_0 \approx (0.17)(46\,T^3) \approx 7.8\,T^3. \tag{44}$$

In the sQGP, it is customary to give the viscosity per entropy density, which for an ideal massless QGP is

$$s_0 = \frac{4\pi^2}{90}\left[16 + \left(\frac{7}{8}\right) \times 2 \times 2 \times 3 \times N_f\right] T^3 \approx 20T^3 \tag{45}$$

for three flavors. Correcting a bit for a more realistic lattice entropy, we will use $s \approx 23\,T^3$ around $T = 1.5Tc$. Thus, the dimensionless viscosity $\eta \approx 0.17$ as measured in this one-species cQGP at $\Gamma \approx 3$ can be translated to the dimensionfull viscosity in the sQGP by rescaling through η_0. The viscosity per entropy ratio in the sQGP is

$$\frac{\eta}{s} \to \frac{\eta\,\eta_0}{s} \approx 0.34. \tag{46}$$

The results from $N = 4$ supersymmetric Yang-Mills theory have suggested a universal lower bound for $\eta/s \geqslant 1/4\pi$. Our

analysis suggests that in the sQGP this ratio is about four times the lower bound. At the same time it is much smaller than the weak coupling result $\eta/s \sim 1/\alpha_s^2 > 1$.

The diffusion constant translates to

$$D \approx 0.161 \rightarrow (0.161)(\lambda^2/\tau_0) \approx 0.1/T. \quad (47)$$

Similarly, the stress-tensor decorrelation time translates to

$$\tau_\eta \approx 0.395 \rightarrow (0.395)(\tau_0) \approx 0.08/T. \quad (48)$$

One should keep in mind that these results are estimated for $T \approx 1.5T_c$. As temperature gets closer to T_c, the masses of quasiparticles grow further and the coupling gets larger, so one finds even stronger coupled plasma. Unfortunately, we do not yet have sufficiently precise lattice data to make the mapping of the cQGP to the sQGP in this region more definite.

V. CONCLUSIONS AND OUTLOOK

Quarks and gluons in the temperature range of (1–1.5) T_c behave as quasiparticles with masses larger than $m > 3\,T$ and a Casimir-weighted Coulomb strength of the order of $\langle C\,\alpha_s \rangle \approx 1$, which is strong. Lattice measured potentials in this temperature range give $\Delta U/T$ between 20 at T_c and 5 at $1.2T_c$, indicating the dominance of the potential energy over the thermal energy.

In this paper, we have suggested that the long-wavelength properties of the QGP in the (1–1.5) T_c range may be modeled by a classical and nonrelativistic gas of massive quasi-particles interacting via strong but classical color charges. This model (cQGP) was studied using molecular dynamics simulations.

Our results show the existence of several phases ranging from a gas phase at weak coupling, through a liquid phase at intermediate coupling, and finally a crystal-like phase at strong coupling with antiferromagnetic-like color ordering. The transition from liquid to crystal is best seen in the density-density correlation function or its static counterpart, the structure function. At large Coulomb coupling the excess energy per particle approaches the Madelung energy for a crystal.

We have used numerical analysis to extract a number of transport coefficients, including the quasiparticle diffusion constant, the shear viscosity, and relaxation time. Although quantum mechanics is important in the sQGP in the formation of the underlying quasiparticles (dispersion laws) and the running of the coupling, we have suggested that the ensuing quasiparticle interaction and dynamics are essentially Coulombic and classical at strong coupling. For this, the cQGP results are generic at intermediate and strong coupling. We have given qualitative arguments for how to relate the cQGP transport results to those of interest in the sQGP by identifying the pertinent length scales. We have found that the sQGP corresponds to $\Gamma \approx 3$, which is liquid-like and has a viscosity $\eta/s \approx 1/3T$.

In subsequent papers, we will provide more insights into the cQGP results presented here for the bulk thermodynamics, two-particle correlations, and transport properties.

ACKNOWLEDGMENTS

This work was partially supported by US-DOE Grant Nos. DE-FG02-88ER40388 and DE-FG03-97ER4014.

[1] E. V. Shuryak, Phys. Lett. **B78**, 150 (1978); Yad. Fiz. **28**, 796 (1978); Phys. Rep. **61**, 71 (1980).
[2] E. Braaten and R. D. Pisarski, Nucl. Phys. **B337**, 569 (1990).
[3] D. Teaney, J. Lauret, and E. V. Shuryak, Phys. Rev. Lett. **86**, 4783 (2001); arXiv:nucl-th/0110037; P. F. Kolb, P. Huovinen, U. Heinz, and H. Heiselberg, Phys. Lett. **B500**, 232 (2001); P. F. Kolb and U. Heinz, in *Quark Gluon Plasma 3*, edited by R. C. Hwa and X.-N. Wang (World Scientific, Singapore, 2004).
[4] E. Shuryak, Prog. Part. Nucl. Phys. **53**, 273 (2004).
[5] E. V. Shuryak and I. Zahed, Phys. Rev. C **70**, 021901(R) (2004); Phys. Rev. D **70**, 054507 (2004).
[6] M. Asakawa and T. Hatsuda, Nucl. Phys. **A715** 863c (2003); S. Datta, F. Karsch, P. Petreczky, and I. Wetzorke, Phys. Rev. D **69**, 094507 (2004).
[7] S. Ichimaru, H. Iyetomi, and S. Tanaka, Phys. Rep. **149**, 91 (1987).
[8] K. Johnson, Ann. Phys. (NY) **192**, 104 (1989).
[9] S. K. Wong, Nuovo Cimento A **65**, 689 (1970).
[10] J. P. Hansen and I. R. McDonald, Phys. Rev. A **11**, 2111 (1975).
[11] B. A. Gelman, E. V. Shuryak, and I. Zahed, Phys. Rev. C **74**, 044909 (2006).
[12] P. Petreczky, F. Karsch, E. Laermann, S. Stickan, and I. Wetzorke, Nucl. Phys. Proc. Suppl. **106**, 513 (2002).
[13] J. Liao and E. V. Shuryak, Phys. Rev. D **73**, 014509 (2006).
[14] O. Kaczmarek, S. Ejiri, F. Karsch, E. Laermann, and F. Zantow, Prog. Theor. Phys. Suppl. **153**, 287 (2004).